Detection of ultrasonic motion of a scattering surface by photorefractive InP:Fe under an applied dc field

Philippe Delaye

Industrial Materials Institute, National Research Council of Canada, 75 de Mortagne, Boucherville, Québec J4B 6Y4, Canada, and Institut d'Optique Théorique et Appliquée, Unité de Recherche Associée 14 au Centre National de la Recherche Scientifique, Bat. 503, Centre Scientifique d'Orsay, B.P. 147, 91403 Orsay Cedex, France

Alain Blouin* and Denis Drolet

Industrial Materials Institute, National Research Council of Canada, 75 de Mortagne, Boucherville, Québec J4B 6Y4, Canada

Louis-Anne de Montmorillon and Gérald Roosen

Institut d'Optique Théorique et Appliquée, Unité de Recherche Associée 14 au Centre National de la Recherche Scientifique, Bat. 503, Centre Scientifique d'Orsay, B.P. 147, 91403 Orsay Cedex, France

Jean-Pierre Monchalin

Industrial Materials Institute, National Research Council of Canada, 75 de Mortagne, Boucherville, Québec J4B 6Y4, Canada

Received July 26, 1996; revised manuscript received January 30, 1997

The characteristics of an interferometric system based on two-wave mixing at 1.06 μm in photorefractive InP:Fe under an applied field for the detection of ultrasonic motion of a scattering surface are described. A theoretical analysis of possible configurations for the detection of small phase modulation in the undepleted-pump approximation is presented. Experimental assessment of the device for both cw and pulse regimes is performed: The sensitivity, the étendue, the response time, and the behavior under ambient vibrations or moving inspected samples are provided. This adaptive device presents many features appropriate for industrial inspection and compares advantageously with the passive confocal Fabry–Perot device that is now widely used. © 1997 Optical Society of America [S0740-3224(97)00507-9]

1. INTRODUCTION

The optical detection of transient surface motion has many practical applications that include, in particular, the vibration monitoring of engineering structures (aircraft, power plants, etc.) and the detection of ultrasound produced by piezoelectric transducers or by pulsed-laser excitation. The last-named application, usually called laser ultrasonics, in which ultrasound is generated and detected by lasers, presents many advantages over conventional piezoelectric-based methods.[1,2] First, laser ultrasonics is a remote-sensing technique. Consequently it can be used, for example, for inspecting hot materials and products moving on a production line. Second, surfaces of complex shape can also be probed easily. For many applications these advantages compensate for the usually lower sensitivity of the laser-based technique compared with piezoelectric transduction.

One detects an ultrasonic wave or vibration by sending a probe beam onto the surface in motion. This ultrasonic motion induces in turn a phase variation on the beam scattered by the surface. The device used for the detection of ultrasound should be designed to convert this phase variation into an amplitude variation, i.e., to perform phase demodulation on the scattered beam. This task has been usually performed by passive interferometers, the most useful being the confocal Fabry–Perot interferometer operated in a transmission or reflection mode.[3]

Passive interferometers for the detection of surface motion can be advantageously replaced by active or adaptive interferometers based on two-wave mixing (TWM) in photorefractive crystals. The use of photorefractive crystals in adaptive interferometers for telecommunication coherent homodyne receiving[4] and for the detection of the ultrasonic motion of scattering surfaces is now well known.[5–9] The approaches used are based on the classical setup of two-beam coupling in photorefractive crystals. In this scheme two beams, a pump beam and a probe beam, which carries the ultrasonic information in the form of a small phase modulation, interfere in the crystal and create through the photorefractive effect an index grating that reproduces the illumination pattern. The two beams are then diffracted by the grating that they have created. Thus, in the direction

0740-3224/97/0701723-12$10.00

of the probe beam, we have creation of a local-oscillator beam that has the same spatial structure as the probe beam, independently of its speckle structure. Therefore this TWM approach can also be seen as real-time holography. Finally, the probe beam transmitted by the crystal interferes on the detector with the local-oscillator beam to perform phase demodulation and to give a signal proportional to the surface displacement. A useful property of this approach is its large throughput or étendue, which can be defined as the product of the effective cross section of the beam on the crystal by the solid angle subtended by the rays of maximum inclination with respect to the axis.[10] This large étendue originates from the adaptive wave-front properties of the TWM.

For a photorefractive interferometer to be used for ultrasonic detection in most industrial conditions, the grating buildup time should meet the following conditions. First, it should be sufficiently long to generate the reference beam properly, and it should be short enough to limit the sensitivity of the interferometer to low-frequency ambient vibrations and adapt itself to the rapid change in the speckle pattern when the inspected product is moving or the inspected location is changed. An additional reason for a short response time is to permit the use of a pulsed laser. The high peak power of pulsed lasers usually compensate for the losses associated with the scattering and absorbing surfaces. In practice these requirements mean a value of the response time of $\sim 10\ \mu$s. The first crystals to be employed, $BaTiO_3$, quickly showed the limitations of their slow response times that render the devices highly sensitive to vibrations.[5] Consequently, to improve response time, setups that use photorefractive semiconductors were developed.[6] However, these semiconductor crystals have low values for their electro-optic coefficients, which results in weak photorefractive two-beam coupling gain. A known method to increase photorefractive coupling is to apply an external electric field to the crystal.[11] The impossibility of applying a uniform electric field to a GaAs crystal, because of the field-enhanced recombination on the EL2 defect,[12–14] led us to use another kind of III–V photorefractive material, semi-insulating iron-doped indium phosphide (InP:Fe), upon which a uniform dc field can be applied, resulting in an enhancement of the photorefractive effect. We note that a photorefractive beam mixer based on the use of InP under an applied electric field has already been considered.[15] However, the application and the requirements were quite different from ours.

The principle of the technique, as well as the photorefractive parameters of the InP:Fe crystal used and the results obtained with a basic experimental setup, is presented in Section 2. We show that the experimental results are in excellent agreement with the theoretical predictions and confirm the potential of our approach. In Section 3 we discuss various possible configurations for the device and compare their respective advantages and drawbacks for optical detection of ultrasound. Finally, in Section 4 we present the implementation of our approach in a practical system, which satisfies the requirements for industrial use.

2. PHASE DEMODULATION BASED ON PHOTOREFRACTIVE InP:Fe

A. Principle of Phase Demodulation

The demodulation of the phase information encoding an optical beam is based on the TWM mechanism. Two beams, a phase-modulated signal beam $[E_d(0, t)]$ and a pump beam, interfere in a photorefractive crystal (Fig. 1). They create an index of refraction grating through the photorefractive effect that is a replica of the illumination pattern. The two beams are then diffracted by this grating, leading to the creation, in the direction of the transmitted signal beam, of an unmodulated local oscillator (diffracted pump beam) that has the same phase structure as the signal beam and interferes with it. We are then in the usual configuration of homodyne detection, except that in this case the incident beam (signal beam) can have any structure and the field of view of this setup is not limited by the antenna theorem.[16] When the period or the duration of the phase modulation is much smaller than the response time of the photorefractive effect, the photorefractive grating can be considered stationary and the phase of the local oscillator considered constant. Then the amplitude of the transmitted signal beam can be written, in the undepleted-pump approximation,[17] as

$$E_d(x, t) = \exp\left(-\frac{\alpha x}{2}\right) E_d(0, 0)\{[\exp(\gamma x) - 1] + \exp[i\varphi(t)]\}, \quad (1)$$

where the incident signal beam amplitude is $E_d(0, t) = E_d(0, 0)\exp[i\varphi(t)]$. In this expression α is the absorption of the crystal, x is the thickness of the crystal, and γ is the photorefractive amplitude gain.[11,17] The first of the two terms in braces in Eq. (1) represents the diffracted pump (the local oscillator). The second term is the transmitted signal beam. Note that in general γ is a complex quantity, the modulus of which represents the strength of the diffraction grating, whereas its phase is associated with the spatial phase shift between the index-of-refraction grating and the illumination grating. For example, in the case of a photorefractive grating in the diffusion regime[11] the photorefractive gain γ is purely

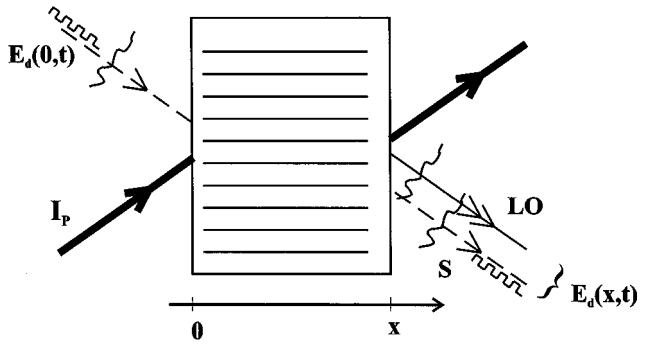

Fig. 1. Principle of phase demodulation by TWM in a photorefractive crystal: a phase-modulated signal beam $E_d(0, t)$ and a pump beam I_p interfere inside the photorefractive crystal to produce an index-of-refraction grating: a local oscillator beam (LO) is diffracted by this grating and interferes with the transmitted phase-modulated signal beam to give a demodulated signal.

real and corresponds to a $\pi/2$ phase shift between the index grating and the illumination grating.

In the limit of a low value of phase modulation $\varphi(t) \ll \pi/2$ {i.e., $\cos[\varphi(t)] \approx 1$ and $\sin[\varphi(t)] \approx \varphi(t)$}, Eq. (1) allows us to calculate the intensity of the signal beam after the crystal:

$$I_d(x, t) = \exp(-\alpha x) I_d(0, 0)[\exp(2\gamma' x) + 2\exp(\gamma' x)\sin(\gamma'' x)\varphi(t)], \quad (2)$$

where $\gamma = \gamma' + i\gamma''$. We can see from Eq. (2) that the photorefractive effect in the diffusion regime (which corresponds to $\gamma'' = 0$) results in a local oscillator in phase with the signal beam and zero sensitivity to small-amplitude phase modulation. As in the case of any interferometer, linear and maximum sensitivity is obtained when the local oscillator and the signal beams are in quadrature. In the drift regime, i.e., with an applied field, the phase between the local oscillator and the signal beam is naturally near or in quadrature. In addition, the use of an applied electric field increases the coupling constant, which results in a more intense local oscillator.

B. Photorefractive InP:Fe under a dc Field

Indium phosphide is a III–V material that is made semi-insulating by iron doping. Its photorefractive properties are now well known, even if particular aspects are still subjects of discussion.[18–21] The sample that we used in these experiments is of the same origin and has the same characteristics as the one we previously characterized.[20] The iron total concentration is $\sim 10^{17}$ cm^{-3}. The dimensions of the crystal are 7.52 mm $\times$ 4.56 mm $\times$ 4.93 mm along directions [110], [001], and [$\bar{1}$10], respectively, and the interaction length is 4.93 mm. The absorption of the sample is $\alpha = 2.13$ cm^{-1}, and the dark resistivity is 5×10^7 Ω cm. We measured an intensity photorefractive gain in the diffusion regime $\Gamma = 0.24$ cm^{-1} for a grating spacing $\Lambda = 0.78$ μm. To describe its photorefractive behavior we used the model that takes into account the excited state of Fe^{2+},[20] using the same parameters as those of the crystal studied previously (i.e., $[Fe^{2+}] = 3.2 \times 10^{15}$ cm^{-3}).

C. Experimental Setup

We implement the two-beam coupling setup described in Fig. 1. The two beams are obtained from a 500-mW single-mode cw diode-pumped Nd:YAG laser emitting at 1.064 μm. In the signal beam pathway we introduce an electro-optic modulator that creates the phase modulation. In most experiments the phase modulation is sinusoidal with frequency ν and with amplitude $\varphi_0 = 135$ mrad. A high voltage is applied to silver-painted electrodes on the [001] faces of the crystal. The strong pump beam is expanded for uniform illumination of the crystal and a uniform electric field inside the crystal. Both beams enter the crystal by the [$\bar{1}$10] face. The incident illumination is 1.6 W cm^{-2}. The signal is detected by a silicon photodiode, which has a quantum efficiency $\eta = 0.3$.

The angle between the two beams is 11°, which corresponds to a grating spacing $\Lambda = 5.5$ μm. This spacing does not correspond to an optimum value to maximize the photorefractive gain. Indeed, the angle between the beams should be rather small to maximize the gain, whereas a large angle gives the large étendue that is necessary when one is working with beams affected by speckle, which is the case for the practical applications that we are considering. The angle that we have chosen actually results from a compromise between these two requirements.

The last experimental issue is the application of the dc voltage. The photoconductivity of InP:Fe is important, and with high illumination levels a high current is produced, causing crystal heating. The main effect of this heating is to increase the conductivity, which in turn increases the current, accelerating heating until destruction of the crystal occurs. To reduce heating of the crystal we apply the high voltage only during the small period of time during which we make the measurement. The typical duration used for field application is $\sim$10 ms at a repetition rate of 1 Hz. This duration is sufficiently long compared with the crystal response time, so steady state is reached before the end of the electrical pulse. This approach was found successful, and no measurable heating of the crystal was observed during application of an electric field. This approach is also justified by the fact that ultrasound is generally detected by laser pulses of small duration (a few tens of microseconds) and low repetition rates (1–100 Hz), so it is quite appropriate to apply the electric field only during the time needed for detection. The applied voltage varies between 0 and 3200 V, which corresponds to electric fields up to 7 kV cm^{-1}.

D. Experimental Results

The application of a dc field causes two effects on the photorefractive gain; first, it increases the modulus of the gain, and second, it shifts the space-charge field grating back toward the illumination grating. For high fields (however, not too high, to avoid being in the trap saturation regime) this results in an index grating that is in phase with the illumination grating. The real part of γ is responsible for a small energy transfer as expressed by the first term of Eq. (2), whereas the imaginary part of γ is responsible for the transformation of the phase modulation into an intensity modulation, as indicated by the second term of Eq. (2). Therefore, by measuring at the same time the values of the energy transfer and of the modulation amplitude, one can determine the real and the imaginary parts of the photorefractive gain. The results are shown in Fig. 2, where we show the rapid increase of the imaginary part of γ and the smaller increase of the real part.

Another important characteristic of the present device is its frequency response, which corresponds to that of a high-pass filter with a cutoff frequency linked to the time constant τ_0 of the photorefractive effect. Measurements were performed for three values of the applied electric field, and the results are presented in Fig. 3. The increase of τ_0 with the applied dc field causes the observed shift of the frequency cutoff. Furthermore, we see on the curve corresponding to the highest field a small overshoot in the frequency response curve near 2 kHz. This overshoot decreases at lower fields. To confirm that the frequency response is dependent on the photorefractive time

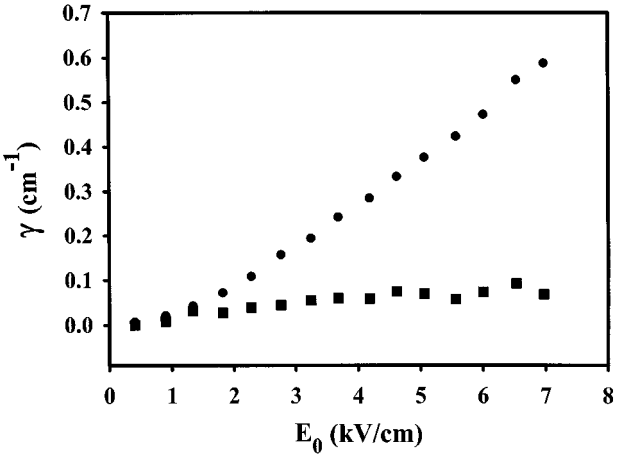

Fig. 2. Photorefractive gain amplitude (■, real part; ●, imaginary part) as a function of the applied electric field.

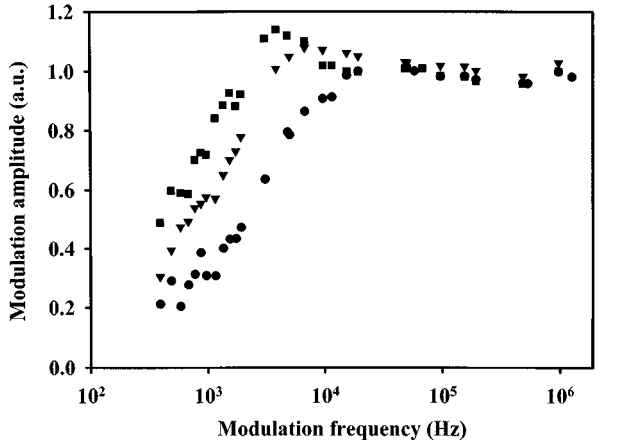

Fig. 3. Frequency response of the photorefractive beam mixer for three different applied electric fields: (●, 2.3 kV cm^{-1}; ▼, 4.6 kV cm^{-1}; ■, 7 kV cm^{-1}). The experimental curves are normalized to their high-frequency values.

constant, we obtained this time constant by measuring the energy transfer kinetics. Without phase modulation applied to the signal beam, we measured the transient variation of the output signal intensity when the pump was rapidly cut off. The results are plotted in Fig. 4. To describe the kinetic behavior we use a model of photorefractive two-beam coupling in presence of absorption[17] that provides the following expression for the variation of the amplitude of the transmitted signal beam (the grating begins to be written at time $t = 0$):

$$E_d(x, t) = \exp\left(-\frac{\alpha x}{2}\right)\exp(\gamma x)E_d(0, 0) \times \left[\tau_0 H(x, t) + \int_0^t H(x, T)\mathrm{d}T\right], \quad (3)$$

with

$$H(x, t) = \frac{\exp(\gamma x)}{\tau_0} \times \exp\left(-\frac{t}{\tau_0}\right) {}_1F_1\left\{\frac{\gamma}{\alpha}, 1, \left[\frac{\exp(\alpha x) - 1}{\exp(\alpha x)}\right]\frac{t}{\tau_0}\right\},$$

where ${}_1F_1(a, b, z)$ is the confluent hypergeometric function. We fitted this expression to the data of Fig. 4 by using the gain value previously measured, $\gamma = (-0.08 - 0.58i)$ cm^{-1}. From this fit we found for the time constant the value $\tau_0 = (31 + 48i)$ μs.

With this determination of the time constant all the parameters are now known, so we can calculate theoretically the frequency response of the photorefractive demodulation device. We use the model mentioned above, which takes into account the absorption of the crystal[17] to derive the amplitude at the output of the crystal:

$$E_d(x, t) = \exp\left(-\frac{\alpha x}{2}\right)\exp(\gamma x)\left\{E_d(0, 0) + \int_0^t\left[\tau_0\frac{\partial E_d}{\partial t}(0, T) + E_d(0, T) - E_d(0, 0)\right]H(x, t - T)\mathrm{d}T\right\}, \quad (4)$$

where $E_d(0, t) = E_d(0, 0)\exp[-i\varphi_0 \sin(2\pi\nu t)]$ is the phase-modulated amplitude at the input of the crystal. Using Eq. (4) and the values of τ_0 and γ previously determined, we can readily calculate the frequency response of the device, which is plotted in Fig. 5 with experimental data. The agreement between the experimental and the calculated curves is good. All the features observed experimentally are well predicted by the model, including the cutoff frequency and the position and height of the overshoot. The agreement is not so good at low frequencies, but this range corresponds to values at which the signal is low and the steady-state value is not completely reached because the electric field is applied only during limited time intervals.

The values of the gain and of the time constant determined in our experiments are also in good agreement with the theoretical values determined by the model of the photorefractive effect in InP:Fe that takes into account the excited state of Fe^{2+}.[20] Using this model and the parameters given in Ref. 20, we determine, for a grating spacing of 5.5 μm, an illumination of 1.14 W cm^{-2} (corrected for reflection losses at the entrance of the crystal) and a field of 7 kV cm^{-1}, a gain $\gamma_{\mathrm{th}} = (-0.35 - 0.84i)$ cm^{-1}, and a time constant $\tau_{0\mathrm{th}} = (29$

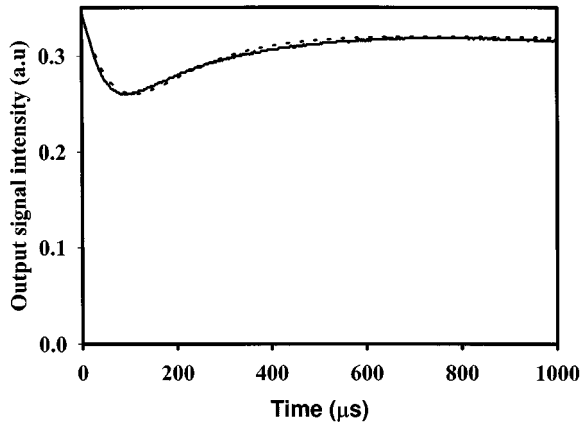

Fig. 4. Kinetics of the transient energy transfer (solid curve) with its theoretical fit (dashed curve).

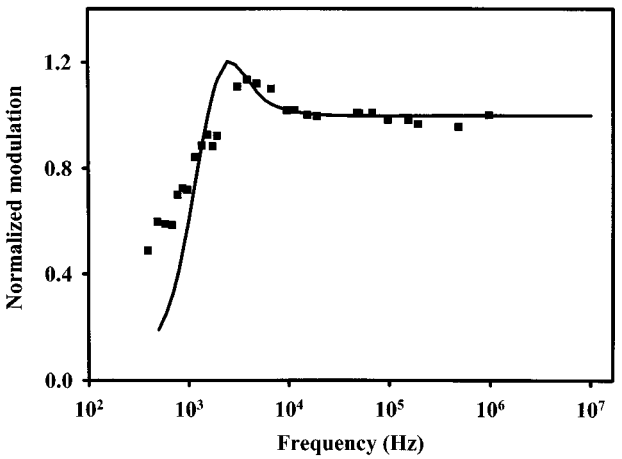

Fig. 5. Theoretical (curve) and experimental (■) frequency-response curves for an applied electric field of 7 kV cm^{-1}.

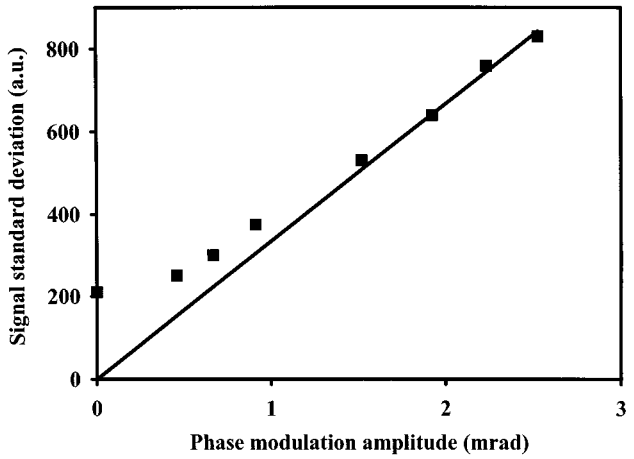

Fig. 6. Demodulated signal standard deviation (■) as a function of the amplitude of the phase modulation; the straight line is a guide for the eye.

$+ 65i)$ μs. These values are in reasonable agreement with the values that we have measured, i.e., $\gamma_{\text{exp}} = (-0.08 - 0.58i)$ cm^{-1} and $\tau_{0\,\text{exp}} = (31 + 48i)$ μs.

E. Sensitivity of the Device

To characterize our system fully we have to determine its responsiveness and the smallest phase amplitude that it can detect. We measure first the standard deviation of the received signal as a function of the phase-modulation amplitude (Fig. 6). The signal is sinusoidally phase modulated at a frequency of 5 MHz, the intensity incident upon the detector is 0.3 mW, and the electrical signal is filtered with a filter bandwidth of 15.5 MHz centered at 8 MHz. The crystal is used in the same condition as indicated above, with an applied electric field of 7 kV cm^{-1}. We see from Fig. 6 that the signal varies linearly with the phase-modulation amplitude and that at low values of the phase-modulation amplitude the observed signal becomes dominated by noise, which is essentially of photonic origin in the experimental conditions of the measurement. From these data we estimate the smallest detectable displacement (displacement that is due to an ultrasonic motion that would give a signal equivalent to the photonic noise) to be 35 pm (rms value). Taking into account the absorption of the crystal, we estimate the intensity incident upon the crystal to be 0.9 mW (the reflection losses are not taken into account, as they can be eliminated by antireflection coatings). So, for a normalized intensity (1 W) and a normalized bandwidth (1 Hz), we obtain a limit of detection: $\delta_l = 2.7 \times 10^{-7}$ nm$\sqrt{\text{W/Hz}}$ for the ultrasonic displacement.

This limit can also be calculated theoretically from Eq. (2). The standard deviation of the signal is then given by

$$S = \frac{\eta A I_{d0}}{h\nu}(2\varphi)\exp(-\alpha x)\exp(\gamma' x)\sin\ \gamma'' x, \tag{5}$$

whereas photon noise is given by the following expression:

$$N = \left[2\frac{\eta A I_{d0}}{h\nu}\Delta f\ \exp(-\alpha x)\exp(2\gamma' x)\right]^{1/2}, \tag{6}$$

which gives a signal-to-noise ratio of

$$\text{S/N} = \left(2\frac{\eta A I_{d0}}{h\nu\Delta f}\ \varphi\right)^{1/2}\exp\left(\frac{-\alpha x}{2}\right)\sin\ \gamma'' x. \tag{7}$$

In Eqs. (5)–(7), η is the quantum efficiency of the detector, A is the area of the detector, $AI_{d0} = AI_d(0, 0)$ is the power incident upon the crystal, Δf is the electronic bandwidth, the photorefractive gain is still $\gamma = \gamma' + i\gamma''$, and φ is the measured rms value of the phase modulation. In the case of the detection of ultrasonic motion, this phase modulation is linked to the rms value of the ultrasonic displacement δ by $\varphi = (4\pi\delta)/\lambda$, $h\nu$ is the photon energy, and λ is the wavelength of the beams.

The limit of detection, which corresponds to a signal-to-noise ratio of 1 and which is normalized to an electronic bandwidth of 1 Hz and an incident power of 1 W, is given by the following expression deduced from Eq. (7):

$$\delta_l = \frac{\lambda}{4\pi}\left(\frac{h\nu}{2\eta}\right)^{1/2}\frac{\exp\left(\frac{\alpha x}{2}\right)}{\sin\ \gamma'' x}. \tag{8}$$

Using the parameters of the experiment, we then calculate $\delta_{l\,\text{th}} = 2.8 \times 10^{-7}$ nm $\sqrt{\text{W/Hz}}$ which is found to be in excellent agreement with the experimental value.

F. Conclusion

We have shown in this study that a photorefractive InP:Fe crystal under an applied dc field can be used as a phase demodulator. Good sensitivity was obtained, even though the crystal parameters and the applied voltage were not optimum. The use of a crystal with lower absorption would lead to even better sensitivity. It is anticipated that the use of another type of crystal with a higher electro-optic coefficient, such as photorefractive CdTe:V, would permit higher values of γ'' and consequently increased sensitivity to be obtained.

3. CONFIGURATIONS FOR PHOTOREFRACTIVE PHASE DEMODULATION

In the direct scheme used above we showed that, in the case of an index grating that is not $\pi/2$ phase shifted, it is

possible after square-law detection by an optical detector at the output of the crystal to transform the phase modulation into an intensity modulation. We now present different configurations of the setup that work with $\pi/2$ phase-shifted gratings or more generally with any phase-shifted grating, discuss their performances, advantages, and drawbacks, and use this analysis to compare GaAs and InP:Fe as phase demodulators.

A. Direct Detection

We have shown that when a phase-modulated signal beam is used in a two-beam coupling setup, the transmission of the signal beam through the photorefractive crystal is given by Eq. (2). The signal-to-noise ratio of the demodulated output is then

$$\mathrm{S/N} = \left(\frac{2\eta A I_{d0}}{h\nu\Delta f}\right)^{1/2} \varphi \exp\left(-\frac{\alpha x}{2}\right) \sin \gamma'' x. \tag{9}$$

Equation (9) shows that the grating has to be at least partly local (in the sense of not shifted toward the illumination grating) to perform phase demodulation. In the case of a photorefractive material this occurs only with an applied dc electric field (or eventually in presence of the photovoltaic effect, a case that does not occur with semiconductors). From Eq. (9) we see that the value of the signal-to-noise ratio is maximum in this case for a moderate value of the gain ($\gamma'' x = \pi/2$). This setup is then advantageous and simple to implement if a local grating of moderate efficiency can be obtained.

B. Isotropic Diffraction Setup

The isotropic diffraction setup was first described in Ref. 5. It uses the two-beam coupling scheme and two polarization components (Fig. 7). In front of the crystal, a half-wave plate (HWP) rotates the incident s-polarized signal beam polarization by 45° and creates s- and p-polarized phase-modulated components of equal intensity. The s-polarized component interferes with the s-polarized pump beam to create a photorefractive grating upon which the two s-polarized components diffract to generate the two-beam coupling energy transfer [according to Eq. (1)]. At the same time the p-polarized component is transmitted undisturbed (except by absorption of the crystal). On leaving the crystal, the signal beam goes through a phase plate (phase shift φ_L) with neutral axes along the s and p directions. The two phase-shifted components are then combined by a polarizing beam splitter (PBS) oriented at 45° to the s and p directions and sent onto two detectors, yielding two signals, S_x and S_y, that are finally electronically subtracted by a differential amplifier. The value of the difference signal $S = S_x - S_y$ is given by the following expression [when $\varphi(t) \ll \pi/2$]:

$$S = \exp(-\alpha x) I_d(0,0)\{\exp(\gamma' x)\cos(\varphi_L - \gamma'' x) + \varphi(t) \times[\sin \varphi_L - \exp(\gamma' x)\sin(\varphi_L - \gamma'' x)]\}, \tag{10}$$

where $\gamma = \gamma' + i\gamma''$ is still the photorefractive gain. The wave-plate phase shift φ_L can be chosen to optimize the factor of $\varphi(t)$. This optimized value is $\varphi_L = (\pi/2) + \mathrm{Arg}[\exp(\gamma x) - 1]$, and then we have in this case

$$S = \exp(-\alpha x) I_d(0,0)[\cos(\varphi_L) + |\exp(\gamma x) - 1|\varphi(t)]. \tag{11}$$

In the case of a pure photorefractive gain ($\gamma'' = 0$), the maximum value of S is obtained for $\varphi_L = \pi/2$ and is given by $S = \exp(-\alpha x) I_d(0,0)[\exp(\gamma x) - 1]\varphi(t)$. We have then linear phase demodulation in the case of the pure photorefractive grating. In the general case it is always possible to find a wave-plate phase shift that optimizes the amplitude of the demodulated signal, but there will always remain a dc component that unbalances the differential detection.

We now consider the case where $\gamma'' = 0$ to calculate the signal-to-noise ratio. The unmodulated component of the signal on each detector, which is used for the calculation of the noise, is

$$S_0 = \exp(-\alpha x)\,\frac{I_d(0,0)}{4}\,[\exp(2\gamma x) + 1].$$

The signal-to-noise ratio is then given by

$$\mathrm{S/N} = \left(\frac{\eta A I_{d0}}{h\nu\Delta f}\right)^{1/2} \varphi \exp\left(-\frac{\alpha x}{2}\right) \frac{\exp(\gamma x) - 1}{[\exp(2\gamma x) + 1]^{1/2}}. \tag{12}$$

If we remember that the photorefractive two-beam coupling intensity gain is $\Gamma = 2\gamma$ we obtain the expression derived by Blouin and Monchalin in Ref. 6. We see from this expression that the maximum signal-to-noise ratio (obtained in this case for large values of γ) is lower by a factor of $\sqrt{2}$ than that for the direct-detection scheme. The reason for this can be traced to the fact that only half of the intensity of the signal is used to create the photorefractive grating.

This configuration has the advantages of permitting linear detection for a pure photorefractive grating and of providing a differential output. In the case of a grating with any phase shift we lose the differential output feature but maintain the setup's linear detection. The maximum signal-to-noise ratio is lower than that obtained with the direct-detection scheme. All the advantages of both approaches are brought together by a third approach that uses the phenomenon of anisotropic diffraction that exists in photorefractive crystals.

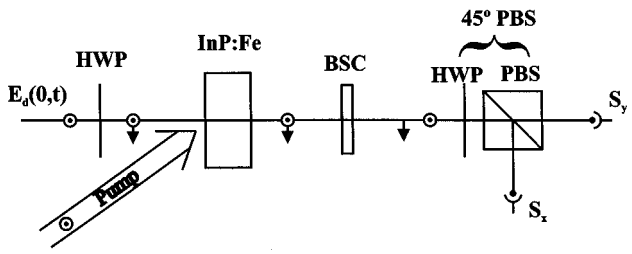

Fig. 7. Schematic of the isotropic diffraction setup: BSC, Babinet–Soleil compensator.

C. Anisotropic Diffraction Setup

In the anisotropic diffraction configuration, which is close to the one that we have just discussed, the s- and p-polarized beams at the output of the crystal are the transmitted and the diffracted beams, respectively. In this case there is no need for a half-wave plate before the crystal to produce the p-polarized beam as in the isotropic

diffraction setup. This effect of diffraction with perpendicular polarization, called anisotropic diffraction, is possible in photorefractive materials because of the tensorial properties of the electro-optic effect.[22] For example, in $\bar{4}3m$ semiconductors such as InP and GaAs, anisotropic diffraction occurs when $[\bar{1}10]$ is the input face, [001] is the incidence plane, and the signal and the pump beams are *s* polarized along [001].[23] The grating vector is then oriented along the [110] direction and the diffracted beam is *p* polarized in the [001] plane.[22,24] This anisotropic diffraction configuration, as shown below, permits linear phase demodulation and a differential output for any phase shift of the grating.

In the approximation of low diffraction efficiency (undepleted-pump approximation), the amplitudes of the two components in the direction of the transmitted signal beam are

$$E_{dS}(x,\,t) = E_d(0,\,0)\exp[i\varphi(t)]\exp\left(-\frac{\alpha x}{2}\right),$$

$$E_{dP}(x,\,t) = \gamma x E_d(0,\,0)\exp\left(-\frac{\alpha x}{2}\right). \tag{13}$$

The *s*-polarized transmitted beam $E_{dS}(x,\,t)$ is phase modulated, whereas the *p*-polarized diffracted beam $E_{dP}(x,\,t)$ is not. After the crystal, the setup is the same as in the case of isotropic diffraction, and the same type of calculation gives, for the differential output,

$$S = -2\exp(-\alpha x)I_d(0,\,0)\{|\gamma|x\,\cos[\varphi(t) + \varphi_L - \varphi_\gamma]\}, \tag{14}$$

where here $\gamma = |\gamma|\exp(i\varphi_\gamma)$ is the photorefractive gain. The optimum phase shift for linear detection is such that $|\varphi_L - \varphi_\gamma| = \pi/2$. In this case S is equal to

$$S = 2\exp(-\alpha x)I_d(0,\,0)|\gamma|x\varphi(t). \tag{15}$$

Equation (15) shows that it is always possible to adjust the phase plate to get, at the same time, optimum sensitivity and a balanced differential output, independently of the grating phase shift. In the case of a pure photorefractive grating the optimum phase shift is $\varphi_L = \pi/2$ and could be given by a quarter-wave plate. In the case of a local grating the optimum phase shift is 0, and there is no need for a wave plate.

In the general case, the unmodulated part of the signal incident upon each detector is

$$S_0 = \exp(-\alpha x)\,\frac{I_d(0,\,0)}{2}\,(|\gamma|^2x^2 + 1)$$

which gives for the signal-to-noise ratio[6]

$$\mathrm{S/N} = \left(\frac{2\eta A I_{d0}}{h\nu\Delta f}\right)^{1/2}\varphi\,\exp\left(-\frac{\alpha x}{2}\right)\,\frac{|\gamma|x}{(|\gamma|^2x^2 + 1)^{1/2}}. \tag{16}$$

The maximum value of the signal-to-noise ratio that can be obtained is then the same as in the case of direct detection, but it is obtained in the limit of high values of the modulus of the photorefractive gain. The advantage of the anisotropic diffraction scheme is that the signal-to-noise ratio depends on the gain's modulus and not only on its imaginary part. Furthermore, this detection scheme allows for differential detection independently of the grating phase shift, which is advantageous when one is working with high-power pulses, as we explain below.

The previous calculation assumed that the crystal was isotropic, which is the case for $\bar{4}3m$ crystals when no electric field is applied. When an electric field is applied in the direction of the grating vector along the [110] axis the medium becomes birefringent, with axes oriented at $\pm 45°$ to the [110] direction and indices along these axes $n_0 \pm \Delta n/2$ (with $\Delta n = {n_0}^3 r_{41}E_0$, where E_0 is the applied electric field). It then follows that the calculation performed previously is not valid anymore. We perform a new calculation by first projecting the light fields onto these new axes. By taking into account the phase shift introduced by the birefringence $\varphi_E = (2\pi\Delta n x)/\lambda$ and noting that there are two waves polarized along the new axes that are diffracted with opposite photorefractive gain $\pm\gamma$, we obtain for the amplitudes of two components in the direction of the transmitted signal beam the following expressions:

$$\begin{aligned} E_{dS}(x,\,t) = {} & \frac{E_d(0,\,0)}{2}\exp\left(-\frac{\alpha x}{2}\right) \\ & \times (-\{\gamma x - \exp[i\varphi(t)]\}\exp(i\varphi_E) \\ & + \{\gamma x + \exp[i\varphi(t)]\}), \\ E_{dP}(x,\,t) = {} & \frac{E_d(0,\,0)}{2}\exp\left(-\frac{\alpha x}{2}\right) \\ & \times (\{\gamma x - \exp[i\varphi(t)]\}\exp(i\varphi_E) \\ & + \{\gamma x + \exp[i\varphi(t)]\}), \end{aligned} \tag{17}$$

Then, performing the same calculation as in the case of anisotropic diffraction without an applied electric field, we obtain the differential output:

$$\begin{aligned} S = {} & -I_d(0,\,0)\exp(-\alpha x)((|\gamma|^2x^2 - 1)\sin\varphi_E \\ & \times \sin\varphi_L + 2|\gamma|x\{\cos\varphi_L\cos[\varphi(t) - \varphi_\gamma] \\ & - \sin\varphi_L \times \sin[\varphi(t) - \varphi_\gamma]\cos\varphi_E\}), \end{aligned} \tag{18}$$

which gives, in the limit of small displacements,

$$\begin{aligned} S = {} & -I_d(0,\,0)\exp(-\alpha x)[(|\gamma|^2x^2 - 1)\sin\varphi_E \\ & \times \sin\varphi_L + 2|\gamma|x(\cos\varphi_L\cos\varphi_\gamma + \sin\varphi_L \\ & \times \sin\varphi_\gamma\cos\varphi_E) + 2|\gamma|x\varphi(t)(\cos\varphi_L\sin\varphi_\gamma \\ & - \sin\varphi_L\cos\varphi_\gamma\cos\varphi_E)]. \end{aligned} \tag{19}$$

The optimum phase shift of the variable phase plate φ_L is chosen to maximize the amplitude of the $\varphi(t)$ factor, which yields the relation

$$\tan\varphi_L = -\cos\varphi_E\cot\varphi_\gamma. \tag{20}$$

In this case S is given by

$$\begin{aligned} S = {} & -I_d(0,\,0)\exp(-\alpha x)\Big[\sin\varphi_E \\ & \times \sin\varphi_L(|\gamma|^2x^2 - 1 - 2|\gamma|x\tan\varphi_E\sin\varphi_\gamma) \\ & + 2|\gamma|x\varphi(t)\,\frac{\sin\varphi_\gamma}{\cos\varphi_L}\Big]. \end{aligned} \tag{21}$$

Equation (21) shows that in general a dc level is left. Furthermore, the maximum of the signal is reduced with respect to the case without birefringence. Nevertheless, in the case of a local grating, as often occurs under an applied electric field, this expression is further simplified. In this case $\varphi_\gamma = \pi/2$, which results in $\tan \varphi_L = 0$, $\varphi_L = 0$, and the following expression for S:

$$S = -2I_d(0, 0)\exp(-\alpha x)|\gamma|x\varphi(t), \tag{22}$$

which is the expression without dc offset found previously in the case of no birefringence [Eq. (15)]. Therefore in this case of an applied electric field the birefringence induced by the Pockels effect does not usually decrease the performance of the anisotropic diffraction configuration.

D. Comparison of the Various Configurations

All the expressions for the signal-to-noise ratio found for the three configurations analyzed above can be put into the form

$$\mathrm{S/N} = \left(\frac{2\eta A I_{d0}}{h\nu\Delta f}\right)^{1/2} \varphi \exp\left(-\frac{\alpha x}{2}\right)\mathrm{SF}, \tag{23}$$

where the sensitivity factor (SF) depends on the configuration. We calculated the sensitivity factor for the three configurations as a function of the photorefractive gain, and the results are plotted in Fig. 8 for a crystal length of 1 cm. The three curves are plotted as a function of the same gain parameter, which differs according to the configuration used: the imaginary part of the gain for direct detection, the real part of the gain for isotropic diffraction, and the modulus of the gain for anisotropic diffraction. Even if some caution is exercised in the interpretation of these results, they confirm that direct detection has the highest SF. However, note that anisotropic diffraction leads to a value of SF of approximately the same magnitude as that obtained by direct detection and furthermore has the advantage of a balanced differential output. Another advantage of anisotropic diffraction compared with the other configurations, which is not directly obvious from the curves of Fig. 8, is that its sensitivity is proportional to the modulus of the gain, which is obviously greater than both its imaginary and its real parts. The anisotropic diffraction configuration consequently uses the photorefractive gain more efficiently. It should also be noted that the curves of Fig. 8 compare the performances of a given crystal (of a given length and given absorption) in different configurations for variable gain. In practice, for a given crystal the absorption and the gain are determined, the latter being fixed by the grating period and the maximum electric field that could be applied safely to the crystal. In this case there is an optimum length that maximizes the signal-to-noise ratio and beyond which a higher value of SF is canceled by a higher value of the absorption factor [see Eq. (23)]. Therefore optimum use of a given crystal requires having the crystal cut as closely as possible to its optimum length.

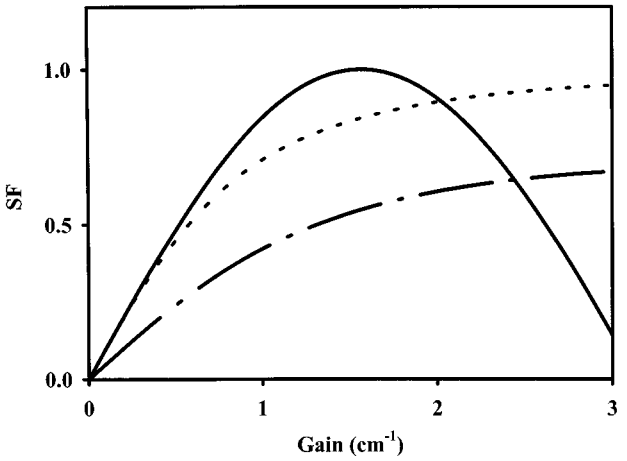

Fig. 8. Sensitivity factor as a function of the gain (curves calculated for a crystal thickness of 1 cm) for the various configurations: direct detection (solid curve), isotropic diffraction (dotted–dashed curve), and anisotropic diffraction (dashed curve).

We now use the anisotropic diffraction setup to compare the performances of GaAs (in the diffusion regime) that have been reported[6] and of InP:Fe (in the drift regime). Using the same InP:Fe crystal as before but now with the electrodes on the [110] faces, we measure a limit of detection equal to $\delta_l = 5.5 \times 10^{-7}$ nm $\sqrt{\mathrm{W/Hz}}$. This value is two times lower than the value previously obtained in the direct-detection setup, in part because of the greater interelectrode distance in this configuration for this crystal, which leads to a smaller value of the applied electric field and consequently to a smaller value of the gain ($|\gamma| = 0.3$ cm^{-1}). For this value of the gain we calculate a theoretical value $\delta_{l\mathrm{th}} = 5.4 \times 10^{-7}$ nm $\sqrt{\mathrm{W/Hz}}$ in excellent agreement with the experimental value. For GaAs we are in the diffusion regime, so we use the same setup with a greater angle between the beams to be at the optimum grating spacing. The grating phase shift is compensated for by a quarter-wave plate. We measured a limit of detection equal to $\delta_l = 4.7 \times 10^{-7}$ nm $\sqrt{\mathrm{W/Hz}}$. The photorefractive gain in this configuration is $\gamma' = 0.27$ cm^{-1}, the absorption 1.55 cm^{-1}, and the crystal thickness is 1 cm. The theoretical limit is then calculated as $\delta_{l\mathrm{th}} = 3.9 \times 10^{-7}$ nm $\sqrt{\mathrm{W/Hz}}$, also in good agreement with the experimental value.

These results, which were obtained with an InP:Fe crystal not optimized with respect to its absorption and length, show that InP:Fe can provide a good performance, matching that obtained with GaAs. The choice of a better crystal with lower absorption and higher gain will allow us to approach the ultimate sensitivity of this kind of demodulator, $\delta_{l\mathrm{th}} = (\lambda/4\pi)\sqrt{h\nu/2\eta} = 4.7 \times 10^{-8}$ nm $\sqrt{\mathrm{W/Hz}}$ (at 1.06 μm and for a quantum efficiency of the detector of 0.3). A factor of 5–10 improvement in performance could therefore be achieved by the choice of a better crystal. The experiment reported next, in a pulsed regime, was performed with a crystal satisfying this requirement.

4. PULSED OPERATION OF THE PHASE DEMODULATOR

All the experiments presented in Sections 2 and 3 were performed in the cw regime and in ideal conditions, with plane waves and with beams of sufficient power. How-

ever, in practice these ideal conditions are rarely encountered; most of the inspected materials have scattering surfaces with low reflecting properties, which means that the returned beam (signal beam) is usually a low-power speckled beam. Furthermore, to have high cutoff frequency (near 10 kHz) we need a high-power pump (10–100 times higher than the one used in the cw regime). Both of these requirements mandate the use of high-power pulse illumination. The photorefractive phase demodulator should therefore be analyzed in this regime, and we should in particular verify that the performances found previously can be extrapolated to high-power pulse operation. In this section we present the results obtained in this regime. In particular, we compare the performance of our InP:Fe phase demodulator with that of another known system now widely accepted, the confocal Fabry–Perot demodulator (CFP). Finally, to test the capacity of the system to adapt rapidly to changes in the incoming wave front, we present measurements performed to observe the effect of large and relatively fast surface motions, which correspond to the case in which the tested object is moving in the direction along the line of sight.

A. Experimental Setup

The laser is a single-mode Nd-YAG laser that delivers 50-μs FWHM pulses with an energy of 100 mJ at a repetition rate of 1–20 Hz. In our system the laser power is split into two beams. The first beam is transmitted to the low-reflecting surface of the test object by a large-core multimode fiber. Another large-core multimode fiber (numerical aperture of 0.39 and core diameter of 1 mm, and thus an étendue of 0.39 mm^2 sr) is used to transmit the collected scattered light to the phase demodulator. The second beam is the pump beam of the TWM setup. To ensure that there will be a few milliwatts of returned power incident upon the photorefractive crystal, most of the laser power is sent onto the inspected material, and only a small part of this beam (less than 10%) is used in the pump beam. The maximum incident peak power of the pump beam is then near 100 W/cm^2. Owing to the pump power used and the sufficiently long pulse duration, the photorefractive grating is fully built at the pulse maximum, so we are in a quasi-steady-state regime at the peak of the pulse, when the measurement is performed.

We apply the electric field only during the duration of the pulse; typically we apply electric field pulses of 170-μs duration and 3200-V amplitude that cover the entire duration of the optical pulse. Although a high current flows across the crystal (because of the high illumination and the high applied voltage), we notice only a small increase in the temperature of the crystal (of $\sim$10 K) at the highest pump peak power (for 100 W/cm^2 and a 10-Hz repetition rate). This increase in temperature is small enough that we can extrapolate the results obtained at lower power to this high-power range. The setup uses the anisotropic diffraction configuration, using a Babinet compensator after the crystal to optimize the signal. The test specimen is usually a carbon epoxy composite material with a rough and black surface; the scattered light is collected by a multimode fiber, as mentioned above. At the output of this fiber we have a signal beam with a high numerical aperture and a speckle structure. The mean grating spacing is $\sim$4 μm (close to the one used in the cw regime) and corresponds to a mean angle between the two beams of $\sim$15°.

We use for these measurements another InP:Fe crystal with a lower iron doping of $1-3 \times 10^{16}$ cm^{-3} to increase the gain-to-absorption ratio. This leads to a crystal with identical photorefractive performances but lower absorption, $\alpha = 0.8$ cm^{-1}. The dimensions of the crystal are 6.6 mm $\times$ 6.6 mm $\times$ 9.95 mm along directions [110], [001], and [$\bar{1}$10], respectively, and the optical thickness is 9.95 mm; the crystal has antireflection-coated input faces. In the cw regime we measure a photorefractive gain $|\gamma| = 0.3$ cm^{-1} and a limit of detection $\delta_{l\mathrm{th}} = 2.7 \times 10^{-7}$ nm $\sqrt{\mathrm{W/Hz}}$ [which is in good agreement with the theoretical value of $\delta_{l\mathrm{th}} = 2.5 \times 10^{-7}$ nm $\sqrt{\mathrm{W/Hz}}$). Therefore we verify that this crystal has a better performance than the one used previously, as expected by its higher gain-to-absorption ratio and its greater interaction length.

B. Sensitivity in the Pulse Regime with a Speckled Signal Beam

To measure the sensitivity of our setup we introduce into the probe beam (before the coupling into the multimode fiber) an electro-optic phase modulator, excited sinusoidally, that produces a phase shift equivalent to a displacement of 2.4 nm over the entire frequency range of interest. For phase-modulated frequencies higher than the low-frequency cutoff ($\sim$10 kHz), the photorefractive response is predicted to be flat, without a high cutoff frequency. We experimentally verified that the response is flat up to 300 MHz, which is the limit of the optical detector used. For the experiments performed to evaluate the sensitivity, we restrained the frequency range to a bandwidth of 15.5 MHz, centered at 8 MHz, using an electronic filter. The noise of the system was essentially photon noise, although there was some residual electronic thermal noise. We performed all the sensitivity measurements by taking into account only the photon noise. For each frequency we measured the signal-to-noise ratio, from which we deduced the limit of detection by taking into account the signal beam power incident upon the crystal (taken after the input polarizer, used to polarize vertically the depolarized beam emerging from the multimode fiber). The result is shown in Fig. 9. As expected, the sensitivity is constant over the whole frequency range, with an absolute value of $\delta_{l\mathrm{th}} = 3.3 \times 10^{-7}$nm $\sqrt{\mathrm{W/Hz}}$, which corresponds to the value obtained in the cw regime with plane waves. This indicates that there is no loss of the sensitivity as the result of use of the multimode fiber. The performance of this photorefractive device was also compared with that of another high-étendue device for ultrasound detection, the CFP interferometer.[3] For this purpose we sent the signal beam into a 1-m-long CFP interferometer used in the transmission mode (mirror reflectivity 85%) and measured the signal-to-noise ratio. The results are also shown in Fig. 9. We see the minimum limit $\delta_{l\mathrm{th}} = 3 \times 10^{-7}$ nm $\sqrt{\mathrm{W/Hz}}$ is approximately the same as the limit obtained with the photorefractive device. This value is also in agreement with the theoretical value,

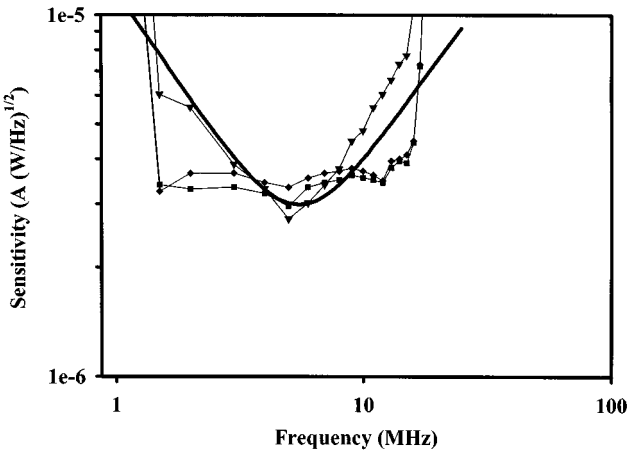

Fig. 9. Sensitivity (limit of detection) of the photorefractive beam mixer based on InP:Fe with an applied electric field (■) and with the CFP interferometer (▼). The bold curve shows the variation of the theoretical sensitivity of the CFP interferometer adjusted to fit the experimental curve. The results obtained with the photorefractive beam mixer where the pump beam issued from a multimode fiber are also shown (♦).

$\delta_{l\mathrm{th}} = 2 \times 10^{-7}$ nm $\sqrt{\mathrm{W/Hz}}$, obtained for an interferometer stabilized at half-height.[3] Figure 9 also shows that the TWM photorefractive interferometer based on InP:Fe under an applied electric field is superior to the CFP interferometer over most of the frequency range under study, reinforcing our interest in this new system. The étendues of both systems are at least equivalent and are limited by the multimode fiber étendue (0.39 mm^2 sr).

C. Photorefractive Phase Demodulator with a Speckled Pump Beam

All the experiments that we have performed so far used a pump beam that is a plane wave. However, the photorefractive effect is not restricted to plane waves. To verify this point we performed an experiment in which we used a large-core multimode fiber (numerical aperture 0.16, core diameter 0.4 mm) to transmit the pump beam. The beam issued from the fiber had a top-hat energy spatial distribution with a superimposed speckled structure, in other words, a wave front very far from a plane wave, with a mean power near 100 $\mathrm{W/cm}^2$. We then performed the same sensitivity measurements as those previously performed with a plane-wavelike pump beam. The results are shown in Fig. 9, and we can conclude that the sensitivity of the TWM phase demodulator is the same in both cases.

The use of a fiber to transmit the pump beam actually has several advantages. First, the demodulator can be set up remotely from the laser, the signal and pump beams both being transmitted by fibers. Second, the top-hat structure given by the fiber provides a more uniform illumination of the crystal than the Gaussian beam, and this is more appropriate when an electric field is applied, as it is the case in our setup. Finally, fibers could permit the use of shorter-coherence-length lasers by easily providing path equalization between interferometric arms.

D. Phase Demodulation from an Inspected Sample in Motion

In several cases of practical interest the object probed by ultrasound is affected by motion or vibrations of the sample. For motion in a direction transverse to the line of sight, the speckle structure of the signal beam is modified. For large enough velocity, the photorefractive grating is unable to follow or adapt itself to the modifications of the speckle pattern, which results in both grating erasure and unmatched reference and signal beams. A detailed analysis of the speckle decorrelation effect is beyond the scope of this paper. For motion in the direction of the line of sight, the velocity causes a Doppler shift of the received light and consequently a displacement of the interference grating. If the response time of the photorefractive effect is sufficiently short, the photorefractive grating will adapt to this displacement and there will be no loss of sensitivity to ultrasonic motion.[25] For longer response time the response will be affected.

We perform the experiment by phase modulating the signal beam at a few megahertz with a low amplitude and giving to it a Doppler frequency shift of known value by mounting the probed sample upon a vibration shaker (which simulates a target with a longitudinal speed v_L). We measure the amplitude of the demodulated signal as a function of this frequency shift ($\Delta f = 2v_L/\lambda$). The frequency shift has two effects on the index grating: It shifts the grating from its steady-state position and it decreases the grating's amplitude. Both effects contribute to a decrease of the demodulated signal, the former effect because the wave-plate phase shift φ_L is not optimum anymore. To analyze these two effects separately we perform two experiments: first, for each frequency shift we compensate for the induced spatial phase shift by changing the wave-plate phase shift φ_L; second, we keep the wave-plate phase shift at its initial value determined without a Doppler shift. The first experiment identifies the decrease in the amplitude of the demodulated signal caused by the decrease in the amplitude of the grating only (see Fig. 10), as well as the variation of the spatial phase shift of the grating. The second experiment yields the contributions of both effects (see Fig. 11). We see from Fig. 10 that the compensated curve is symmetrical, with an axis of symmetry not centered on the zero-frequency shift. For the noncompensated curve (Fig. 11)

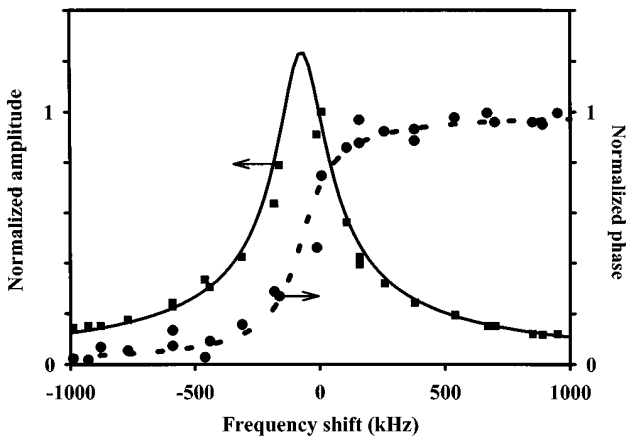

Fig. 10. Normalized amplitude (■) of the demodulated signal and normalized measured phase shift (●) as a function of the Doppler frequency shift, with compensation of the induced phase shift for each Doppler shift. The curves are theoretical fits with a time constant $\tau = (1.1 - 0.8i)\mu$s.

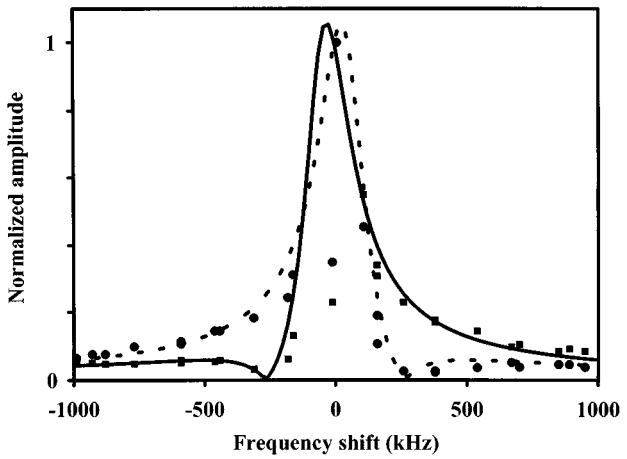

Fig. 11. Normalized amplitude of the phase-demodulation signal as a function of the Doppler frequency shift, without compensation of the induced phase shift, for positive (■) and negative (●) applied electric fields. The curves represent theoretical fits with a time constant $\tau = (1.2 - 0.6i)\mu$s.

the behavior is more complex. The amplitude of the demodulated signal goes to zero for a finite frequency shift; moreover, the curves obtained for applied fields of opposite polarities are symmetric with respect to the zero-frequency-shift axis.

To explain these results we use a simple model. The space-charge field's amplitude is governed by a first-order differential equation[11]:

$$\frac{\partial E_1}{\partial t} = -\frac{1}{\tau_0} E_1 - m \frac{E_{sc}}{\tau_0}, \tag{24}$$

where E_{sc} and τ_0 depend on material parameters and are complex in the case when an electric field is applied.[11,20,26] For this calculation we assume that τ_0 is constant throughout the crystal, which means that we neglect the effects of absorption and of the pulse shape (this assumption is quite reasonable because the measurement is performed at the top of the pulse, where the illumination is fairly constant). We then illuminate the crystal with a moving grating,[27] i.e., a modulation term of the form $m(t) = m_0 \exp(i\Delta\omega t)$, where $\Delta\omega = 2\pi\Delta f$, so we are looking for a field of the form $E_1(t) = E_{10} \exp(i\Delta\omega t)$. We then have immediately

$$E_{10} = \frac{-m_0 E_{sc}}{1 + i\Delta\omega\tau_0}. \tag{25}$$

When the phase shift of the grating is compensated for each frequency shift, because the demodulated signal is proportional to $|\gamma|$ [see Eq. (15)], we can conclude that the demodulated signal varies as $|E_{10}|$, i.e., as

$$|E_{10}| = \frac{m_0|E_{sc}|}{\left\{\left[1-\left(\frac{\text{Im } \tau_0}{|\tau_0|}\right)^2\right] + \left(\Delta\omega - \frac{\text{Im } \tau_0}{|\tau_0|^2}\right)^2 |\tau_0|^2\right\}^{1/2}}. \tag{26}$$

The variation of the signal with the Doppler shift is then expected to be represented by a symmetrical curve centered on Im $\tau_0/|\tau_0|^2$, which corresponds to the results shown in Fig. 10. The same analysis leads to the following expression for the spatial phase shift of the grating:

$$\varphi_{E_{10}}(\Delta\omega) - \varphi_{E_{10}}(0) = -\arctan\left(\frac{\Delta\omega \text{ Re } \tau_0}{1 - \Delta\omega \text{ Im } \tau_0}\right), \tag{27}$$

where $E_{10} = |E_{10}|\exp[i\varphi_{E_{10}}(\Delta\omega)]$ and that corresponds to the variation observed in Fig. 10.

In the case when there is no compensation for the phase shift, the demodulated signal is given by Eq. (14) and is then proportional to $A = |E_{10}|\cos[\varphi_{E_{10}}(\Delta\omega) - \varphi_{E_{10}}(0)]$, where $E_{10} = |E_{10}|\exp[i\varphi_{E_{10}}(\Delta\omega)]$ (note that the phase shift of the grating without the Doppler shift is compensated for by the wave plate). We then obtain for the dependence of the demodulated signal as a function of the frequency shift

$$A = m_0|E_{sc}|\left\{\frac{\left[1 - \left(\frac{\text{Im } \tau_0}{|\tau_0|}\right)^2\right]}{\left[1 - \left(\frac{\text{Im } \tau_0}{|\tau_0|}\right)^2\right] + \left(\Delta\omega - \frac{\text{Im } \tau_0}{|\tau_0|^2}\right)^2 |\tau_0|^2} - \frac{\left(\Delta\omega - \frac{\text{Im } \tau_0}{|\tau_0|^2}\right)\text{Im } \tau_0}{\left[1 - \left(\frac{\text{Im } \tau_0}{|\tau_0|}\right)^2\right] + \left(\Delta\omega - \frac{\text{Im } \tau_0}{|\tau_0|^2}\right)^2 |\tau_0|^2}\right\}. \tag{28}$$

Equation (28) includes a symmetric part and an antisymmetric part, both centered at Im $\tau_0/|\tau_0|^2$, in agreement with the experimental results, as shown in Fig. 11. Data for inverted polarity of the applied field are also plotted in Fig. 11. Inversion of the field polarity simply results in a change of the sign of the imaginary part of the time constant.[11,26]

5. CONCLUSION

We have presented the characteristics of an interferometer based on two-wave mixing in InP:Fe under an applied field for the detection of ultrasonic motion from a scattering surface. The experimental results agree well with the theoretical predictions. The measured characteristics of this device confirm its potential for industrial inspection. The device has also been compared with the confocal Fabry–Perot demodulator that at present is widely used for ultrasound detection. The sensitivities and étendues of the two devices are nearly the same. However, the TWM device is more compact and does not require any external electronic stabilization system against ambient vibrations or thermal drift. TWM also operates in a differential detection scheme, which allows us to eliminate the amplitude fluctuations of the laser or the envelope of the pulse when we are working with a pulsed laser. The TWM device presented a flat frequency response, without notches, up to the cutoff frequency of the detectors, which is particularly advantageous in the region of low ultrasonic frequencies (below 2 MHz). In spite of the improvements brought by TWM, the CFP still has some advantages. In particular, it is not sensitive to

the Doppler shift associated with the velocity of the sample in the direction of the line of sight, as any self-reference interferometer is. This behavior is linked to the short response time of the CFP (typically 0.1 μs for a 1-m-long cavity with a finesse of 10), much shorter than the response time of TWM in semiconductors. This faster response time also results in a greater capacity of adaptation of the CFP to the modification of the speckle pattern collected from an inspected sample moving perpendicularly to the laser beams. This advantage is, however, associated with a higher low-frequency cutoff and a reduced sensitivity to the detection of low ultrasonic frequencies, as mentioned above.

ACKNOWLEDGMENT

Philippe Delaye acknowledges the fellowship provided to him by the Société de Secours des Amis des Sciences.

*Corresponding author: e-mail, alain.blouin@nrc.ca.

REFERENCES

1. C. B. Scruby and L. E. Drain, *Laser-Ultrasonics: Techniques and Applications* (Hilger, Bristol, UK, 1990).
2. J. P. Monchalin, "Progress towards the application of laser-ultrasonics in industry," in *Review of Progress in Quantitative Nondestructive Evaluation*, D. O. Thompson and D. E. Chimenti, eds. (Plenum, New York, 1993), Vol. 12A, p. 495.
3. J. P. Monchalin and R. Héon, "Laser ultrasonic generation and optical detection with a confocal Fabry–Pérot interferometer," Mater. Eval. **44**, 1231 (1986).
4. F. M. Davidson and L. Boutsikaris, "Homodyne detection using photorefractive materials as beamsplitters," Opt. Eng. **29**, 369 (1990).
5. R. K. Ing and J. P. Monchalin, "Broadband optical detection of ultrasound by two-wave mixing in a photorefractive crystal," Appl. Phys. Lett. **59**, 3233 (1991).
6. A. Blouin and J. P. Monchalin, "Detection of ultrasonic motion of a scattering surface by two-wave mixing in a photorefractive GaAs crystal," Appl. Phys. Lett. **65**, 932 (1994).
7. D. M. Pepper, P. V. Mitchell, G. J. Dunning, S. W. McCahon, M. B. Klein, and T. R. O'Meara, "Double-pumped conjugators and photo-induced EMF sensors: two novel, high-bandwidth, auto-compensating, laser-based ultrasound detectors," in *Materials Science Forum* (Transtec, Zurich, Switzerland, 1996), Vol. 210, Part 1, p. 425.
8. M. Paul, B. Betz, and W. Arnold, "Interferometric detection of ultrasound at rough surfaces using optical phase conjugation," Appl. Phys. Lett. **50**, 1569 (1987).
9. P. Delaye, A. Blouin, D. Drolet, and J. P. Monchalin, "Heterodyne detection of ultrasound from rough surfaces using a double phase conjugate mirror, " Appl. Phys. Lett. **67**, 3251 (1995).
10. J. P. Monchalin, "Optical detection of ultrasound," IEEE Trans. Ultrason. Ferroelectr. Freq. Control **33**, 485 (1986).
11. N. V. Kukhtarev, V. B. Markov, S. G. Odulov, M. S. Soskin, and V. L. Vinetskii, "Holographic storage in electrooptic crystals. I. Steady state," Ferroelectrics **22**, 949 (1979); "Holographic storage in electrooptic crystals. II. Beam coupling—light amplification," Ferroelectrics **22**, 961 (1979).
12. M. Kaminska, J. M. Parsey, J. Lagowski, and H. C. Gatos, "Current oscillations in semi-insulating GaAs associated with field-enhanced capture of electrons by the major deep donor EL2," Appl. Phys. Lett. **41**, 989 (1982).
13. H. Rajbenbach, J. M. Verdiell, and J. P. Huignard, "Visualization of electrical domains in semi-insulating GaAs:Cr and potential use for variable grating mode operation," Appl. Phys. Lett. **53**, 541 (1988).
14. G. C. Valley, H. Rajbenbach, and H. J. von Bardeleben, "Mobility–lifetime product of photoexcited electrons in GaAs," Appl. Phys. Lett. **56**, 364 (1990).
15. F. M. Davidson and C. T. Field, "Coherent homodyne optical communication receivers with photorefractive optical beam combiners," J. Lightwave Technol. **12**, 1207 (1994).
16. A. E. Siegman, "The antenna properties of optical heterodyne receivers," Appl. Opt. **5**, 1588 (1966).
17. P. Delaye, L. A. de Montmorillon, and G. Roosen, "Transmission of time modulated optical signals through an absorbing photorefractive crystal," Opt. Commun. **118**, 154 (1995).
18. G. C. Valley, S. W. McCahon, and M. B. Klein, "Photorefractive measurement of photoionization and recombination cross sections in InP:Fe," J. Appl. Phys. **64**, 6684 (1988).
19. G. Picoli, P. Gravey, C. Ozkul, and V. Vieux, "Theory of two-wave mixing gain enhancement in photorefractive InP:Fe: a new mechanism of resonance," J. Appl. Phys. **66**, 3798 (1989).
20. P. Delaye, P. U. Halter, and G. Roosen, "Thermally induced hole–electron competition in photorefractive InP:Fe due to the Fe^{2+} excited state," J. Opt. Soc. Am. B **7**, 2268 (1990).
21. R. S. Rana, D. D. Nolte, R. Stelt, and E. M. Monberg, "Temperature dependence of the photorefractive effect in InP:Fe: role of multiple defects," J. Opt. Soc. Am. B **9**, 1614 (1992).
22. J. C. Fabre, J. M. C. Jonathan, and G. Roosen, "$\bar{4}3m$ photorefractive materials in energy transfer experiments," Opt. Commun. **65**, 257 (1988).
23. T. Chang, A. Chiou, and P. Yeh, "Cross-polarization photorefractive two-beam coupling in gallium arsenide," J. Opt. Soc. Am. B **5**, 1724 (1988).
24. P. Delaye, K. Jarasiunas, J. C. Launay, and G. Roosen, "Picosecond investigation of photorefractive and free carrier gratings in GaAs:EL2 and CdTe:V," J. Phys. (France) III **3**, 1291 (1993).
25. D. Drolet, A. Blouin, C. Néron, and J. P. Monchalin, "Specifications of an ultrasonic receiver based on two-wave mixing in photorefractive GaAs implemented in laser-ultrasonic system," in *Review of Progress in Quantitative Nondestructive Evaluation*, D. O. Thompson and D. E. Chimenti, eds. (Plenum, New York, 1996), Vol. 15, p. 637.
26. F. P. Strohkendl, J. M. C. Jonathan, and R. W. Hellwarth, "Hole-electron competition in photorefractive gratings," Opt. Lett. **11**, 312 (1986).
27. Ph. Refrégiér, L. Solymar, H. Rajbenbach, and J. P. Huignard, "Two-beam coupling in photorefractive $Bi_{12}SiO_{20}$ crystals with moving gratings: theory and experiments," J. Appl. Phys. **58**, 45 (1985).